Int. J. Electrochem. Sci., 15 **(2020)** 9971 – 9980, doi: 10.20964/2020.10.65

International Journal of
ELECTROCHEMICAL
SCIENCE
www.electrochemsci.org

Short Communication

Study on Preparation and Performance of $LiNi_{0.8}Co_{0.1}Mn_{0.1}O_2$ as cathode materials for lithium ion batteries

Mingming Wang, Fangchang Shi, Hongzhou Yang, Cunsi Sun Yanmin Gao[*]

School of Materials Science and Engineering, Jiangsu University of Science and Technology, Jiangsu, Zhenjiang 212003, China
[*]E-mail: JUSTGaoYanmin@163.com

Received: 10 June 2020 / *Accepted:* 3 August 2020 / *Published:* 31 August 2020

Lithium ion battery has the advantages of high working voltage, good cycling performance and environmental friendliness. It is widely used in various battery energy storage devices. High nickel ternary positive electrode materials with α-$NaFeO_2$ type layered crystal structure have become the focus of research in recent years due to their high energy density and good cycling performance. In this paper, $LiNi_{0.8}Co_{0.1}Mn_{0.1}O_2$ high-nickel ternary material was prepared by hydrothermal method, and the properties of the material were determined by phase analysis and electrochemical analysis. and the influence of sintering temperature on the morphology and structure and electrochemical performance of the ternary-type material was investigated. The results show that the optimal process conditions for the precursor mixed lithium sintering are divided into two steps: the first step is calcined at 500℃ for 6h, and the second step is calcined at 800℃ for 8h. Under these conditions, the $LiNi_{0.8}Co_{0.1}Mn_{0.1}O_2$ has the best morphology and the highest crystallinity, and has a specific capacity of 198.5 $mAh \cdot g^{-1}$ at the rate of 0.2 C. After 100 charge and discharge cycles at 0.2 C, the capacity retention rate is still 96.7%.

Keywords: hydrothermal method; lithium ion battery; precursor; $LiNi_{0.8}Co_{0.1}Mn_{0.1}O_2$; cathode material.

1. INTRODUCTION

In recent years, with the development of human civilization and the progress of social industrialization, the environmental pollution caused by the burning of traditional fossil fuels has become increasingly serious. It has become a worldwide concern to find and develop new energy sources with high efficiency, environmental protection and sustainable development. Compared with $LiNi_{0.5}Co_{0.2}Mn_{0.3}O_2$ and $LiNi_{0.6}Co_{0.2}Mn_{0.2}O_2$, $LiNi_{0.8}Co_{0.1}Mn_{0.1}O_2$ has attracted more attention due to its lower cost and higher specific capacity [1-6]. Goodenough's research group first proposed $LiCoO_2$ as a positive electrode material for lithium ion batteries in 1980 [7]. Subsequently, Bell LABS reported the

idea of graphite as a cathode material for batteries [8]. Since then, lithium ion battery technology has been widely used in mobile phones, laptops, cameras and other digital electronic devices.

The performance of lithium ion battery largely depends on the quality of anode materials, while the synthesis of ternary anode materials is generally obtained through mixed sintering of precursor and lithium source. The sintering process of ternary anode materials is generally divided into two steps: pre-sintering and sintering [9,10,11]. The first step of pre-sintering is usually to decompose the precursor and the lithium source, so as to make the subsequent chemical reaction of the composite material more smoothly. The second step of sintering is the chemical reaction stage of the final synthesis of ternary materials. The whole sintering process includes a variety of physical and chemical changes, such as dehydration, multiple reactions, melting, calcination, etc. which means that $LiNi_xCo_yMn_{1-x-y}O_2$ is generated by solid phase reaction between precursor and lithium source at a certain temperature, the process of calcination to obtain the complete crystalline layered $LiNi_xCo_yMn_{1-x-y}O_2$ material. This paper mainly studies the effect of sintering temperature on the properties of synthetic ternary materials.

2. EXPERIMENTAL

2.1. Preparation of precursors

The solution A1 was obtained by weighing 4.8mmol $NiSO_4•6H_2O$, 0.6mmol $CoSO_4•7H_2O$ and 0.6mmol $MnSO_4•H_2O$ in 30mL deionized water by full ultrasonic stirring. 12mmol NaOH was weighed and dissolved in 30mL deionized water. Then 2ml ammonia water was added as the complexing agent to obtain solution A2. A1 and A2 were slowly added dropwise to the continuously stirred polytetrafluoroethylene reaction kettle, fully stirred for 30 min, and then subjected to constant temperature hydrothermal reaction. Then it was washed with alcohol and dried to obtain $Ni_{0.8}Co_{0.1}Mn_{0.1}(OH)_2$;

2.2. Preparation of $LiNi_{0.8}Co_{0.1}Mn_{0.1}O_2$

A certain amount of $Ni_{0.8}Co_{0.1}Mn_{0.1}(OH)_2•nH_2O$ and $LiOH•H_2O$ (molar ratio is 1:1.05) was weighed and fully mixed. It is calcined in a tube furnace in two steps. The first step was sintering at 500 ^{0}C for 6h, and the second step was sintering at 780^{0}C, 790^{0}C, 800^{0}C and 810^{0}C (denoted as S1,S2,S3,S4). The sintering time was 8h, and $LiNi_{0.8}Co_{0.1}Mn_{0.1}O_2$ high-nickel ternary material was finally obtained.

2.3. Battery assembly

The $LiNi_{0.8}Co_{0.1}Mn_{0.1}O_2$ positive electrode material was weighed with conductive SP and binder PVDF in a ratio of 89:6:5, and mixed evenly with NMP as the solvent. The obtained slurry was coated on 4*10cm aluminum foil, and dried in a constant temperature vacuum drying oven at 80℃. After drying, it was cut into round electrode pieces with a diameter of 1cm. A button battery is assembled in a glove box with lithium metal as the negative electrode.

3. RESULTS AND DISCUSSION

Fig. 1. is the XRD pattern of $LiNi_{0.8}Co_{0.1}Mn_{0.1}O_2$ prepared at different sintering temperatures. It can be seen that these samples all have very sharp diffraction peaks at the same peak positions and belong to the R3m spatial group of α-$NaFeO_2$ layered crystal structure. The sample sintered at 800 ^{0}C has the strongest diffraction peak and the highest crystallinity, the (108) and (110) peaks split obviously, which proves that the sample S3 has the best crystallinity.

The cell parameters of $LiNi_{0.8}Co_{0.1}Mn_{0.1}O_2$ were calculated to obtain Table. 1. The analysis of the table data shows that the I(003)/I(104) values of the four groups of samples are far more than 1.2, which proves that the cation mixing degree of the samples is very low and can be ignored. S3 sample has the maximum c/a value, indicating a good layered structure[12]. In addition, in terms of cell volume, S3 sample is slightly smaller than other sample. A smaller cell volume can improve the migration rate of lithium ions, and the smaller the grain size, the purer the crystal phase, and the electrochemical performance of the obtained material will be improved accordingly. The R-factor value of S3 sample also decreased significantly, which further proves that the material produced at 800 ^{0}C has the highest ordering.

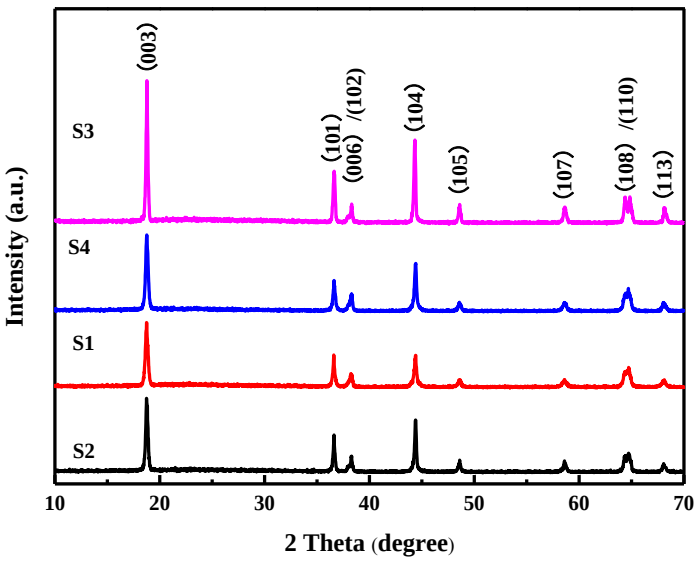

Figure 1. XRD patterns of $LiNi_{0.8}Co_{0.1}Mn_{0.1}O_2$ prepared at different sintering temperatures

Fig. 2 shows the SEM images of $LiNi_{0.8}Co_{0.1}Mn_{0.1}O_2$ prepared at different sintering temperatures. It can be seen that, except for S4 sample, the other three groups of samples all have secondary spherical morphology with a diameter of about 10 μm. The secondary particles are composed of nano-scale primary spherical particles. The morphology of the S4 sample is quite different, this may be caused by high sintering temperature crystal structure is destroyed, the morphology of the material does not favor the transport of ions, lithium ions are subject to greater resistance during insertion and extraction, this will greatly increase the battery internal resistance, electrochemical performance degradation, therefore

should not exceed 810 ^{0}C calcination temperature.

Table 1. Unit parameters of $LiNi_{0.8}Co_{0.1}Mn_{0.1}O_2$ prepared at different sintering temperatures

Sample	a(Å)	c(Å)	c/a	I(003)/I(104)	V(Å^3)	R-factor
S1	2.8805	14.1938	4.9275	2.0000	101.9918	0.4351
S2	2.8782	14.1863	4.9289	1.4065	101.7751	0.4432
S3	2.8723	14.2355	4.9561	1.7051	101.7098	0.3821
S4	2.8801	14.1795	4.9233	1.7802	101.8607	0.6034

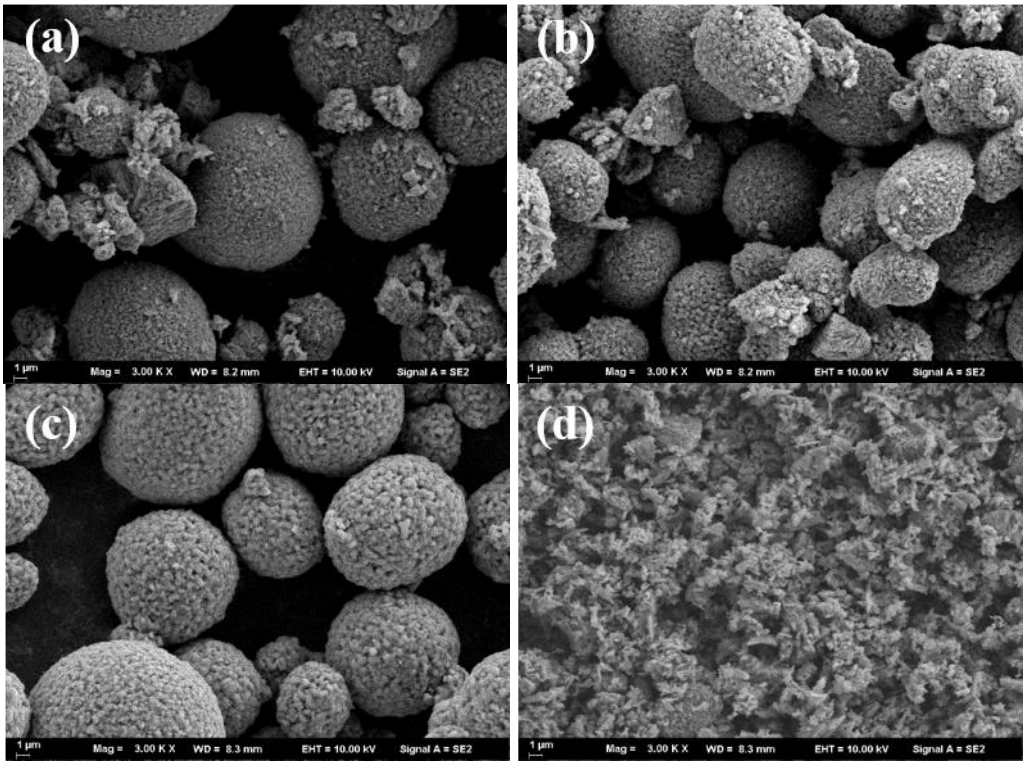

Figure 2. SEM images of $LiNi_{0.8}Co_{0.1}Mn_{0.1}O_2$ prepared at different sintering temperatures a)S1； b) S2； c)S3； d)S4

Therefore, the morphology of ternary positive electrode material will be optimized with the increase of temperature, but once a critical point is exceeded, the crystal structure will be destroyed and the material performance will be greatly reduced. This section concludes that $LiNi_{0.8}Co_{0.1}Mn_{0.1}O_2$ obtained at the sintering temperature of 800 ^{0}C has the optimal morphology.

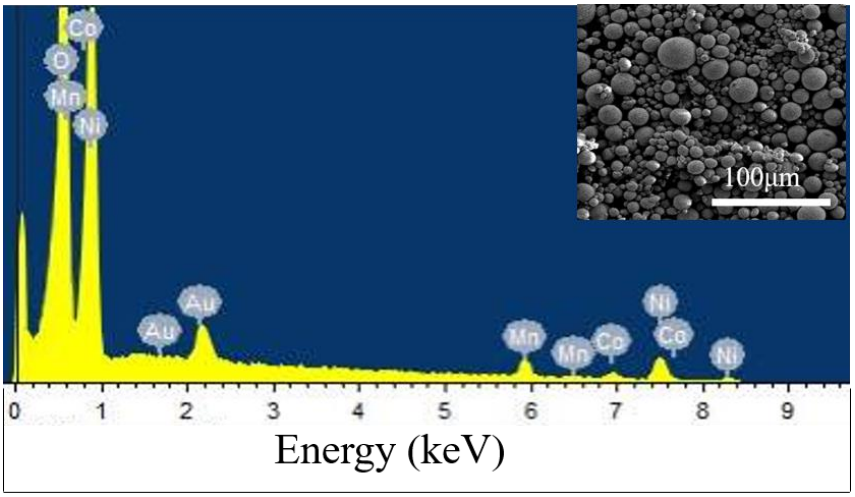

Figure 3. EDS test of $LiNi_{0.8}Co_{0.1}Mn_{0.1}O_2$

Table 2. The element analysis of $LiNi_{0.8}Co_{0.1}Mn_{0.1}O_2$

Element	Weight%	Atomic%
Mn	6.20	10.37
Co	6.20	9.67
Ni	51.07	79.96

Through the phase analysis of $LiNi_{0.8}Co_{0.1}Mn_{0.1}O_2$, it can be known that S3 sample has the best performance in all aspects. Fig. 3 and Table .2. show the EDS test results of ternary material S3 sample. The content ratio of Ni, Co and Mn was 8:0.97:1.03. It can be concluded that the crystal structure of the precursor was not damaged in the sintering process, and the element ratio before and after the synthesis of the ternary material was almost the same, which further proved that the technological condition of calcination at 800 ^{0}C for 8h could combine with the precursor prepared in this paper to prepare $LiNi_{0.8}Co_{0.1}Mn_{0.1}O_2$, a high-nickel ternary anode material with an ideal ratio. Next, the electrochemical properties of ternary anode materials will be analyzed in detail.

S1, S2, S3 and S4 samples are assembled into four groups of button batteries according to the previous method. 5 charging and discharging test cycles were conducted according to the multiplier of 0.1C and voltage range of 3.0-4.5V to activate the battery. After that, the battery performance is analyzed. Fig. 4. is the first charge and discharge curve of $LiNi_{0.8}Co_{0.1}Mn_{0.1}O_2$ prepared at different calcination temperatures under the condition of 0.2C. As the temperature rises, the specific capacities of the first charge and discharge of the materials prepared under the conditions of 780^{0}C, 790^{0}C, 800^{0}C and 810^{0}C calcining are respectively 170.3 mAh·g^{-1}, 190.1 mAh·g^{-1}, 198.5 mAh·g^{-1}, 161.7 mAh·g^{-1}, 161.6 mAh·g^{-1}, 183.3 mAh·g^{-1}, 192.0 mAh·g^{-1} and 153.5 mAh·g^{-1}.

The coulomb efficiencies of S1, S2, S3 and S4 are 94.9%, 96.4%, 96.7% and 94.9% respectively, showing that the precursor reacts well with oxygen during calcination and further optimizes the structure of the material. It can be seen from the Fig.4. Each sample has good charging and discharging

performance because they have a complete charging and discharging platform[13], that the voltage platform is about 3.8V. Both the charge/discharge specific capacity and coulomb efficiency tend to rise first and then fall with the rise of temperature. The sample S3 calcined at 800℃ has the highest initial charge/discharge specific capacity.

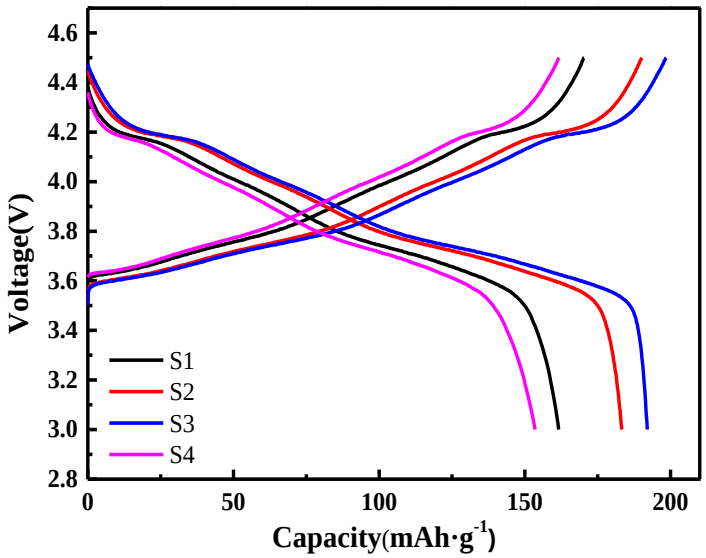

Figure 4. the first charge-discharge curve of $LiNi_{0.8}Co_{0.1}Mn_{0.1}O_2$ prepared at different calcination temperatures at 0.2C

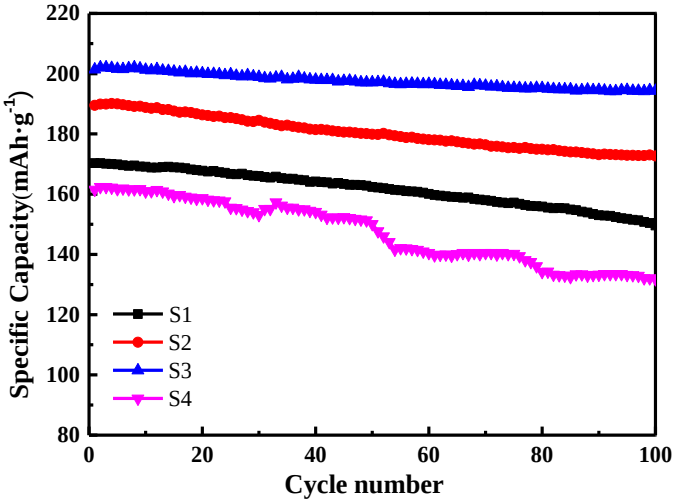

Figure 5. Cycle performance curve of $LiNi_{0.8}Co_{0.1}Mn_{0.1}O_2$ prepared at different calcination temperatures under 0.2C

Fig. 5 shows the cyclic electrochemical properties of S1, S2, S3 and S4. As can be seen from Fig. 5, the capacity of the four battery materials has decreased after 100 cycles, and the attenuation degree varies. After 100 cycles, the discharge specific capacity is 149.6 $mAh \cdot g^{-1}$, 172.7 $mAh \cdot g^{-1}$, 194.3

mAh·g^{-1}, 131.8 mAh·g^{-1} respectively, and the corresponding capacity retention rate is 87.8%, 90.8%, 96.1%, and 81.4%. In addition, the cycling curves of the three samples S1, S2 and S3 can maintain a stable downward trend. With the increase of temperature, the capacity of the battery material prepared keeps the same at each cycle stage. It is proved that when the temperature is below 800℃, the capacity of the material synthesized gradually increases with the increase of the calcination temperature. However, the cycle curve of S4 sample fluctuates greatly, the capacity retention rate is relatively low, and the capacity drops sharply compared with S3 sample. This is because the material structure is destroyed due to the rising temperature, and the cycle stability and capacity of the battery are affected. It can be seen that $LiNi_{0.8}Co_{0.1}Mn_{0.1}O_2$ material synthesized by calcining at 800℃ has the best capacity retention rate and the highest capacity.

As shown in Fig.6, with the increase of current density, the discharge capacity of the battery decreases in step, which is because the increase of current enhances the polarization effect of the battery. After the 2C current discharge, the charging and discharging cycle is carried out again with a small current of 0.2C. It is found that the discharge capacity is lower than the initial capacity, which is because the amount of active lithium decreases after charging and discharging at different current densities. It is also possible that the lattice structure changes, hindering the insertion and extraction of lithium ions, resulting in the degradation of the electrochemical properties of the material. The rate performance of the three samples are gradually improved, and stable discharge capacity can be displayed under different current densities. After the rate performance test for the whole cycle, the capacity of the S3 sample can still reach 189.8 mAh·g^{-1} at 0.2C, and the capacity retention rate reaches 95.1%. This indicates that sample S3 can be applied to a variety of different rate with the best rate performance. Comparing the capacity and the capacity retention rate will find that the performance is better than other similar studies[14,15].On the contrary, the sample S4 performs poorly in the aspect of rate performance, which indicates that too high calcination temperature will lead to the decrease of the rate performance of the material.

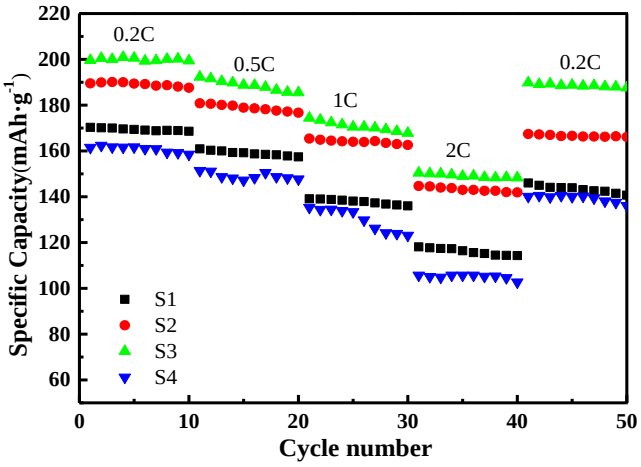

Figure 6. Rate performance graph of $LiNi_{0.8}Co_{0.1}Mn_{0.1}O_2$ prepared at different calcination temperatures

Fig. 7. shows the CV of sample S3, with a voltage range of 2.8-4.5V, scanning three laps at 0.1mv /s. Diagram has obvious oxidation and reduction peaks, this represents a phase transition between the hexagonal phase and monoclinic phase, in addition of the second and third times basic REDOX peak overlap, and slightly lower than the first lap of redox peaks, it represents the polarization effect of lighter materials, and after the polarization phenomenon reduced materials exhibit good reversibility, helps to lithium ion insertion and extraction, makes the stability of the material is getting better.

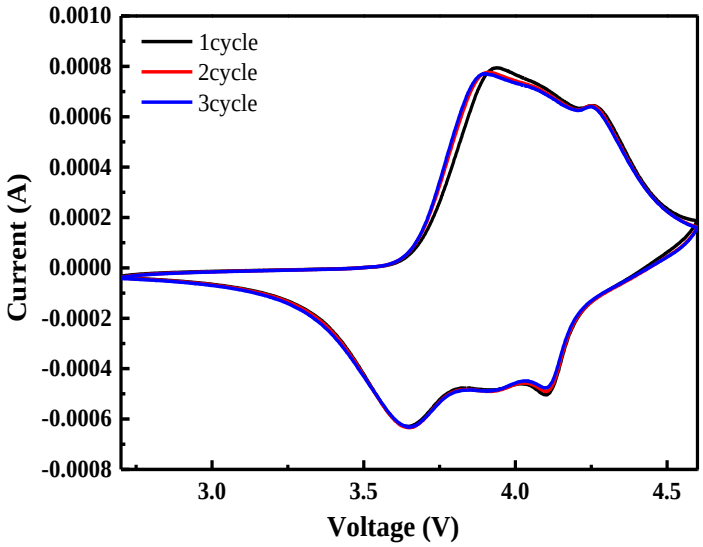

Figure 7. Cyclic voltammetry curve of S3

In the high frequency region of the material's AC impedance spectrum, there is a semicircle, which is generally related to the surface passivation film of the positive electrode material. With the increase of the radius of this semicircle, the resistance of the material interface will increase, while the straight line in the low frequency region reflects the diffusion ability of lithium ions in the material, namely, Warburg impedance [16]. Fig. 8. is the AC impedance spectrum of sample S3. By comparing the impedance plots of the first and 100th turns, the radius of the semicircular arc increased from 25.4Ω to 49.6Ω, indicating that the charge transfer resistance of $LiNi_{0.8}Co_{0.1}Mn_{0.1}O_2$ increases with the cycling process is gradually increasing. This may be due to the electrolyte will react with the electrode material after $LiNi_{0.8}Co_{0.1}Mn_{0.1}O_2$ is removed from lithium. However, it is worth mentioning that the impedance value of $LiNi_{0.8}Co_{0.1}Mn_{0.1}O_2$ material prepared in this paper is very low, and the impedance value increases very little after 100 cycles, which proves that the material has a small charge transfer resistance and good stability.

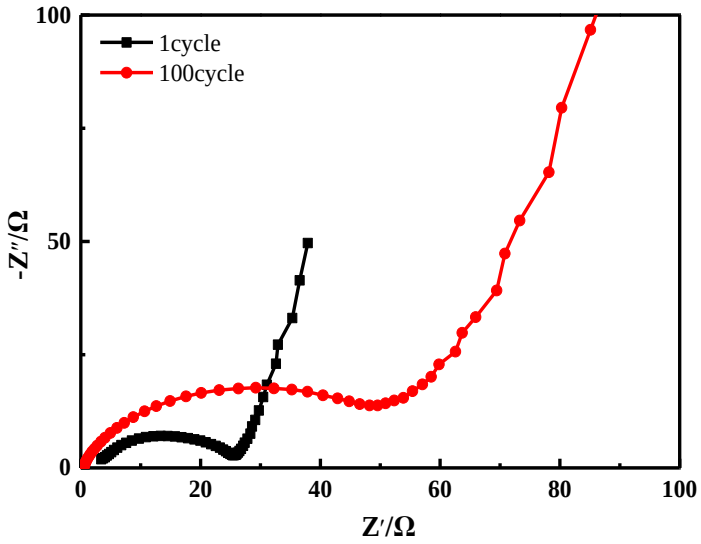

Figure 8. The impedance spectrum of S3

4. CONCLUSIONS

In this work, $LiNi_{0.8}Co_{0.1}Mn_{0.1}O_2$ material was prepared by sintering with $Ni_{0.8}Co_{0.1}Mn_{0.1}(OH)_2$ as the precursor and mixed lithium source $LiOH•H_2O$. Through physical phase analysis and electrochemical analysis, the influence of sintering temperature on the morphology, structure and electrochemical performance of ternaries was investigated. The specific conclusions are as follows: When the calcination temperature is below 800℃, the morphology and electrochemical performance of the ternary materials will improve with the increase of calcination temperature. However, when the reaction temperature exceeds 800℃, the morphology and structure of the materials will be destroyed, the crystallinity will decline, and the electrochemical performance will deteriorate. The calcination temperature of 800℃ is the best temperature. Under this condition, $LiNi_{0.8}Co_{0.1}Mn_{0.1}O_2$ has a specific capacity of 198.5 $mAh \cdot g^{-1}$, and the capacity retention rate is still 96.7% after 100 charge and discharge cycles.

References

1. J. Zheng. W.H. Kan, A.Manthiram, *ACS Appl. Mater. Interfaces*, 7 (2015) 6926-6934.
2. K. Meng, Z. Wang, H. Guo, X. Li, D. Wang, *Electrochim. Acta*, 211 (2016) 822e831.
3. X. Xiong, D. Ding, Y. Bu, Z. Wang, B. Huang, H. Guo, X. Li, *J. Mater. Chem* , 2 (2014) 11691e11696.
4. X. Xiong, D. Ding, Z. Wang, B. Huang, H. Guo, X. Li, *J. Solid State Electrochem* ,18 (2014) 2619e2624.
5. B. Zhang, P. Dong, H. Tong, Y. Yao, J. Zheng, W. Yu, J. Zhang, D. Chu, *J. Alloys Compd* , 706 (2017) 198e204.
6. H. Yang, H. Wu, M. Ge, L. Li, Y. Yuan, Q. Yao, J. Chen, L. Xia, J. Zheng, Z. Chen, J. Duan, K. Kisslinger, X.C. Zeng, W.K. Lee, Q. Zhang, J. Lu, *Adv. Funct. Mater* , 29 (2019) 1808825.

7. K Mizushima, P C Jones, P J Wiseman, *Mater. Res. Bul.l*, 15 (1980) 783-789.
8. B Scrosati, *Electrochim. Acta*, 45 (2000) 2461-2466.
9. M Dong, Z Wang, H Li, *ACS Sustainable Chem. Eng*., 5(11) (2017) 10199-10205.
10. D H Cho, C H Jo, W Cho, *J. Electrochem. Soc.*, 161(6) (2014) A920-A926.
11. K Du, J Huang, Y Cao, *J. Alloys Compd*., 574 (2013)377-382.
12. K. Yang, L. Fan, J. Guo, X. Qu, *Electrochim. Acta*, 63 (2012) 363e368.
13. H. Tian, X. Zhao, J. Zhang, M. Li, H. Lu, *ACS Appl. Energy Mater.*, 1 (2018) 3497-3504.
14. J. Zhou, Q. Wang, M. Zhang, Y. Guo, A. Zhu, X. Qiu, H. Wu, *Electrochimica Acta*, 353 (2020) 136541.
15. F. Ma, Z. Yu, Y. Wu, X. Zhang, C. Lv, J. Qu, *Hydrometallurgy*, 195 (2020) 105370.
16. P P Hsu, D M Sabatini, *Cell*, 134(5) (2008) 707.